Biosensors and Bioelectronics 173 (2021) 112803

Contents lists available at ScienceDirect

Biosensors and Bioelectronics

journal homepage: http://www.elsevier.com/locate/bios

Preparation of PbS NPs/RGO/NiO nanosheet arrays heterostructure: Function-switchable self-powered photoelectrochemical biosensor for H_2O_2 and glucose monitoring

Qingzhi Han, PhD [a,b,c,#], Hanyu Wang [a,b,#], Dan Wu, PhD [a,b,*], Qin Wei, PhD [a,b]

[a] Collaborative Innovation Center for Green Chemical Manufacturing and Accurate Detection, School of Chemistry and Chemical Engineering, University of Jinan, Jinan, 250022, PR China

[b] Key Laboratory of Interfacial Reaction & Sensing Analysis in Universities of Shandong, School of Chemistry and Chemical Engineering, University of Jinan, Jinan, 250022, PR China

[c] Key Laboratory of Theoretical and Computational Photochemistry, Ministry of Education, College of Chemistry, Beijing Normal University, Beijing, 100875, China

ARTICLE INFO

Keywords:
Photoelectrochemical biosensor
H_2O_2 and glucose detection
Self-powered
Function-switchable
PbS NPs/RGO/NiO NSAs

ABSTRACT

On the basis of synthesized PbS nanoparticles (PbS NPs)/reduced graphene oxide (RGO)/NiO nanosheet arrays (NiO NSAs) heterostructure, we constructed a function-switchable self-powered PEC sensing platform for the analysis of H_2O_2 and glucose. Ordered NiO NSAs have high electron mobility, modifying RGO onto the surfaces of NiO NSAs can connect the NiO NSAs with the PbS NPs and promoted the electron transfer rate between them, as well as enhance their photocurrent response. The PbS NPs/RGO/NiO NSAs heterostructure own excellent catalase-like activity can achieve H_2O_2 detection, only with one more step, after introducing glucose oxidase (GOD) onto the surface of PbS NPs/RGO/NiO NSAs heterostructure, we realized the detection conversion between H_2O_2 and glucose. Under optimal conditions, the proposed biosensor exhibited superior analytical performance toward H_2O_2 and glucose, a limit of detection (LOD) of 0.018 mM (S/N = 3) and 5.3×10^{-8} M (S/N = 3) were obtained, respectively. Moreover, good accuracy was obtained in the real samples analysis of H_2O_2 disinfectant and human serum samples.

1. Introduction

Self-powered biosensor (Han et al., 2019; Katz et al., 2001; Li et al., 2019; Luo et al., 2019; Sun et al., 2019; Wu et al., 2019) is a rapidly developed sensing device. For self-powered sensing devices, they need not extra power supply and usually accompanied by redox reaction in the detecting process (Grattieri and Minteer, 2018; Liu et al., 2019; Majdecka et al., 2018; Ouyang et al., 2019; Petromichelaki et al., 2019; Wang et al., 2019). Under light illumination and with the present of analyte, the self-powered photoelectrochemical (PEC) biosensor would give out electrical signal, and need not external energy supply (e.g. battery or plug-in). These characteristics are favorable for the miniaturization and low-cost fabrication of the self-powered PEC biosensor (Zhang et al., 2020). Various materials have been developed for the purpose of self-powered sensing devices, such as Au@BiOI/NiO (Han et al., 2019), PbS/NiO (Dai et al., 2017), CdS/RGO/ZnO (Zhao et al., 2016), CdSe/ZnS/TiO_2 (dos Santos et al., 2018) and RGO/ZnO (Kang et al., 2015). Although some progresses have been made in the field of self-powered PEC bioanalysis, the exploration of new materials/structures for self-powered PEC biosensors have never been stopped.

Nickel oxide (NiO) as a typical p-type semiconductor, owing to its excellent catalytic properties, good stability and unique electrochemical performance, has been wildly used in the field of electrocatalysis (Gong et al., 2014; Nardi et al., 2015), photocatalysis (Liu et al., 2018) and PEC bioanalysis (Dai et al., 2017; Han et al., 2019). What's more, NiO as a p-type semiconductor has a wide band-gap of $Eg = \sim 3.5$ eV (means low visible light absorption), can be a suitable candidate for surface modification of lead sulfide nanoparticles (PbS NPs) (Dai et al., 2017; Han et al., 2019; Liu et al., 2018). PbS NPs possess a narrow band-gap ($Eg = \sim 0.4$ eV) and a large exciton Bohr radius, which make it has high light

* Corresponding authorCollaborative Innovation Center for Green Chemical Manufacturing and Accurate Detection, School of Chemistry and Chemical Engineering, University of Jinan, Jinan, 250022, PR China

E-mail addresses: hqz2941429766@163.com (Q. Han), wudan791108@163.com (D. Wu).

# These authors (#) contributed equally to this work.

https://doi.org/10.1016/j.bios.2020.112803

Received 26 September 2020; Received in revised form 3 November 2020; Accepted 4 November 2020

Available online 7 November 2020

harvest range, high dielectric constant and strong confinement effects of charge carriers (Dai et al., 2017; Mukherjee et al., 2019). Hence, PbS NPs are ideal sensitizer to sensitize p-type NiO NSAs. In order to further promote the PEC performance of the PbS NPs modified NiO NSAs, reduced graphene oxide (RGO) was introduced. As a popular two-dimensional material, RGO coupling with other semiconductors could be used to construct highly efficient photocatalyst or PEC sensing platform (Chi et al., 2019; Han et al., 2018; Jeevitha et al., 2019; Li et al., 2015; Xiang et al., 2015; Zeng et al., 2019). Therefore, RGO as an electron collector was inserted into the middle of PbS NPs/NiO NSAs to form the PbS NPs/RGO/NiO NSAs heterostructure.

Glucose is the power source of cell activity as well as metabolic intermediate product in human body. Hydrogen peroxide (H_2O_2) existed in many biological processes, such as cell apoptosis and protein folding, also is an effective oxidant (Zhang et al., 2015). In the glucose oxidation process, H_2O_2 also is the by-product of the oxidization of glucose (Zhang et al., 2015). With the presence of glucose oxidase (GOD), glucose can be oxidized by oxygen via the following reaction: Glucose + O_2 + H_2O → H_2O_2 + gluconic acid (Han et al., 2019; Wilson and Turner., 1992). Based on this mechanism, the concentration of H_2O_2 could reflect the concentration of glucose. Chen's group realized PEC detection of glucose by using PbS QDs/NiO to compete consuming O_2 with GOD (Dai et al., 2017), while in our design, H_2O_2 as a reactive oxygen species could also take part in the redox reaction of PEC analysis and affect the output signal. Hence, developing a sensing platform for the detection of both H_2O_2 and glucose is feasible.

In this work, NiO NSAs, RGO and PbS NPs were chosen for the construction of self-powered PEC sensing platform. As shown in Scheme 1, firstly, NiO NSAs were modified onto the surface of ITO via hydrothermal reaction and annealing process, secondly, RGO was spin-coated on the surface of NiO NSAs. Following, PbS NPs were in situ formed on the surface of RGO/NiO NSAs via the technique of successive ionic layer adsorption and reaction (SILAR) (Khot et al., 2015). Then, the PEC biosensor for the detection of H_2O_2 was successfully constructed (Scheme 1a), because PbS NPs/RGO/NiO NSAs could decompose H_2O_2 and produce O_2 (Wang et al., 2014; Yu et al., 2015). In order to realize the quantitative analysis of glucose, GOD as an enzyme model was further fixed on the surface of PbS NPs/RGO/NiO NSAs electrode (Scheme 1b). Therefore, based on the PbS NPs/RGO/NiO NSAs heterostructure and by controlling the presence or absence of GOD, we constructed a function-switchable sensing platform for the self-powered detection of H_2O_2 and glucose.

2. Experimental section

Chemicals and apparatus, synthesis of the materials, the detection process, the simulation parameters of the equivalent circuit components, and the analytical performance of the proposed sensing platform compared with various methods for the analysis of H_2O_2 and glucose are offered in the Supporting Information.

3. Results and discussion

3.1. Characterization of NiO NSAs, RGO/NiO NSAs and PbS NPs/RGO/NiO NSAs

Fig 1A clearly depicted the scanning electron microscopy (SEM) image of NiO nanosheet arrays (NSAs), and the NiO nanosheet with a length about ~3 μm. After RGO were modified on NiO NSAs (Fig. 1B) the surface became rough. With the further addition of PbS NPs (Fig. 1C) via SILAR method, the PbS NPs were fixed onto the surface of RGO/NiO NSAs. Fig. 1D showed the transmission electron microscopy (TEM) image of PbS NPs, which has a diameter about ~16 nm. The crystal structures of NiO NSAs, RGO/NiO NSAs and PbS NPs/RGO/NiO NSAs were investigated by XRD measurement (Fig. 1E). The XRD pattern of NiO NSAs possessed sharp diffraction peaks at 37° , 43° , 62° , 75° , 79° corresponding to JCPDS Card No. 47–1049. The XRD pattern of RGO/NiO NSAs compared with NiO NSAs showed one more little peak at 22° (*), which could attribute to the small content of RGO in the RGO/NiO NSAs heterostructure. The XRD pattern of PbS NPs/RGO/NiO NSAs

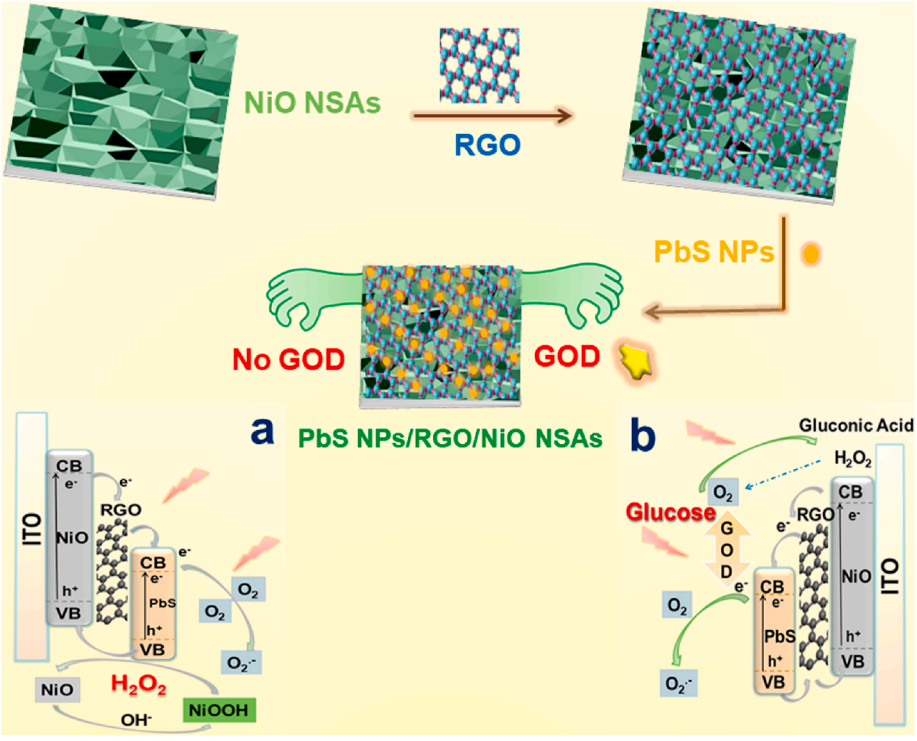

Scheme 1. Schematic illustration of the preparation of PbS NPs/RGO/NiO NSAs heterostructure based platform: application for (a) H_2O_2 and (b) glucose detection, respectively.

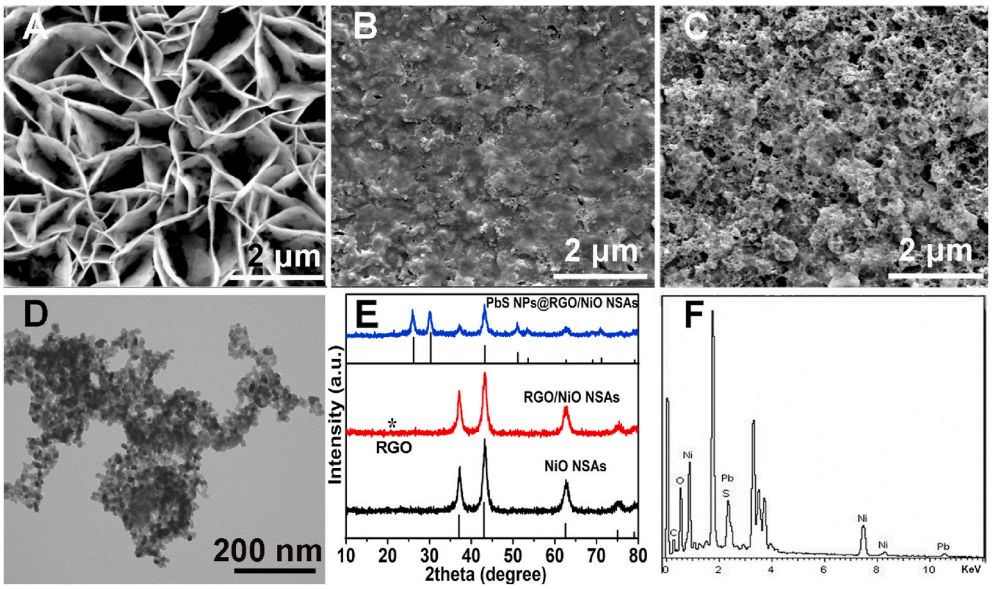

Fig. 1. SEM image of (A) NiO NSAs, (B) RGO/NiO NSAs, and (C) PbS NPs/RGO/NiO NSAs. (D) TEM image of PbS NPs. (E) XRD patterns of PbS NPs/RGO/NiO NSAs, RGO/NiO NSAs and NiO NSAs, respectively. (F) EDS analysis of PbS NPs/RGO/NiO NSAs.

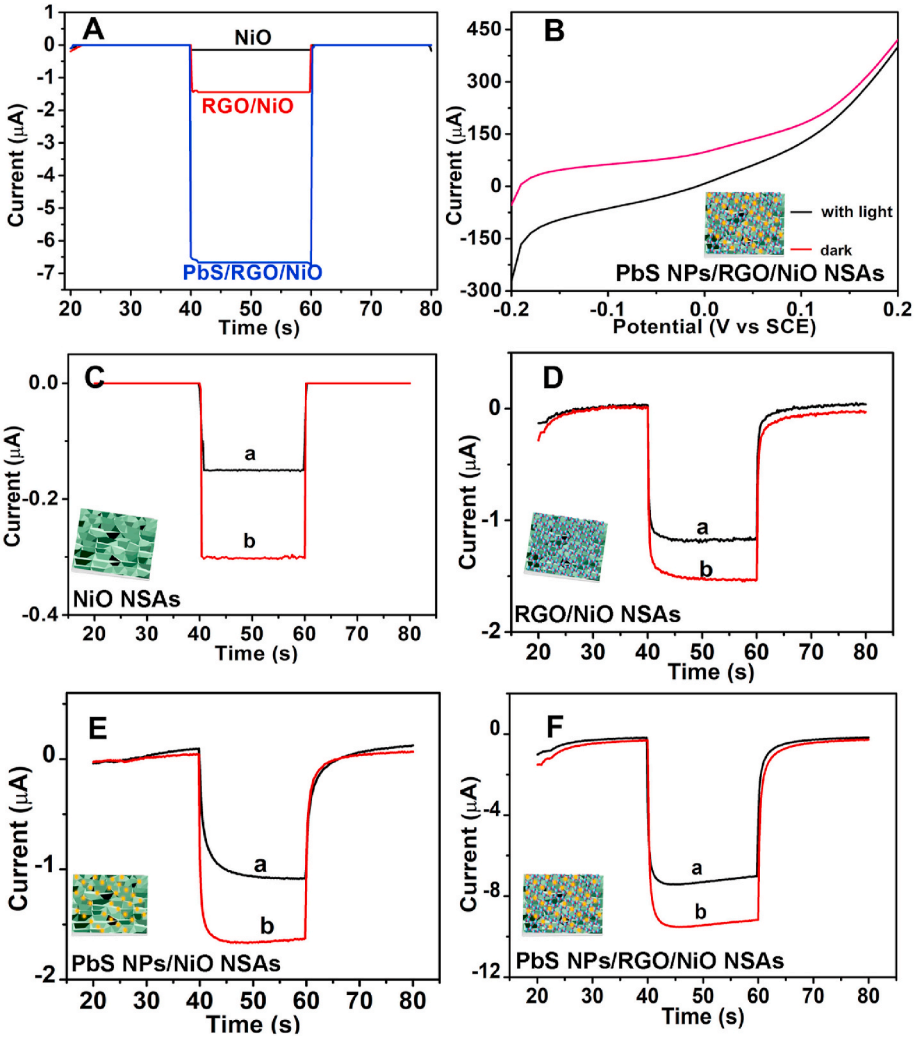

Fig. 2. (A) Photocurrent performance of NiO NSAs (black curve), RGO/NiO NSAs (red curve), and PbS NPs/RGO/NiO NSAs (blue curve) electrodes in air-saturated 0.1 M Tris-HCl solution (pH = 7.0) (with 0 V bias voltage vs. SCE and a 420–430 nm LED lamp-house). (B) The current-potential characteristics of PbS NPs/RGO/NiO NSAs with or without light in the applied range of −0.2–0.2 V. The photocurrent responses of (C) NiO NSAs, (D) RGO/NiO NSAs, (E) PbS NPs/NiO NSAs, (F) PbS NPs/RGO/NiO NSAs without (a) or with (b) the addition of 0.1 mM H_2O_2 (in 0.1 M Tris-HCl buffer, pH = 7.0). (For interpretation of the references to colour in this figure legend, the reader is referred to the Web version of this article.)

showed sharp diffraction peaks at 26°, 30°, 43°, 50° and 53° corresponding to JCPDS Card No. 05–0592, indicating the successful fabrication of PbS NPs/RGO/NiO NSAs heterostructure. The energy dispersive spectrometer (EDS) image (Fig. 1F) of PbS NPs/RGO/NiO NSAs showed the existence of Pb, S, C, Ni and O, which in accordance with its constituents.

X-ray photoelectron spectroscopy (XPS) analysis was also used to investigate the valence states of the C, Ni, O, Pb and S elements in the PbS NPs/RGO/NiO NSAs hybrid nanocomponents. Fig. S1A (Supporting Information) was the XPS survey of PbS NPs/RGO/NiO NSAs, which shows the existence of C 1s, Ni 2p, O 1s, Pb 4f and S 2p. C 1s (284.6 eV) in Fig. S1B could be attributed to RGO and the absorbed CO_2 from air. The high-resolution XPS spectra of Ni 2p (Fig. S1C) shows several peaks in the range of 851–885 eV. The peaks in ~ 853, ~ 860 and ~872 eV are assigned to Ni $2p_{3/2}$ and Ni $2p_{1/2}$, respectively, which could attribute to the NiO compound. O 1s spectrum (Fig. S1D) showed two peaks located at ~ 529 and 531 eV, respectively, could be assigned to Ni–O bond and oxygen-containing groups in RGO. Fig. S1E depicted that the Pb $4f_{7/2}$ and Pb $4f_{5/2}$ peaks located at ~137 and 142 eV. While the S 2p signals (Fig. S1F) consist of S $2p_{1/2}$ and S $2p_{3/2}$ at ~ 160 eV, which could be attributed to the PbS compound.

3.2. PEC characterization

Photocurrent measurement was carried out in a three-electrode configuration with a Pt wire as the counter electrode, saturated calomel electrode (SCE) as the reference electrode and a slide of modified ITO as the working electrode. To investigate the PEC performance of different electrode, we tested the photocurrent responses of the NiO NSAs, RGO/NiO NSAs and PbS NPs/RGO/NiO NSAs electrode, respectively. As shown in Fig. 2A, the PbS NPs/RGO/NiO NSAs electrode exhibited the maximum current ~ −7 μA, which proved the superiority of the PbS NPs/RGO/NiO NSAs heterostructure. The linear sweep voltammetry (LSV) was carried out in both dark and irradiation conditions to investigate the effect of light (Fig. 2B). In the selected range (−0.2–0.2 V), with or without light irradiation the photocurrent both increased, which means the PEC response of PbS NPs/RGO/NiO NSAs enhanced its cathodic photocurrent. The PEC activities of different combination of materials also were investigated, the photocurrent responses of NiO NSAs, RGO/NiO NSAs, PbS NPs/NiO NSAs and PbS NPs/RGO/NiO NSAs without (a) or with (b) the presence of 0.1 mM H_2O_2 in 0.1 M Tris-HCl were depicted in Fig. 2C, D, 2E and 2F. It is obvious that the PbS NPs/RGO/NiO NSAs exhibited the highest photocurrent increment, which indicating the PbS NPs/RGO/NiO NSAs heterostructure is favorable for H_2O_2 detection.

The fabrication steps of the GOD modified electrode was certified via the corresponding photocurrent responses (Fig. 3A) and the EIS Nyquist plots (Fig. 3B). After the addition of RGO and PbS NPs onto the surface of NiO NSAs, the photocurrent responses gradually increased (Fig. 3A, blue curve), which could be attributed to the good electron conductivity of RGO as well as the expanded light absorption range brought by PbS NPs, respectively. With the further modification of GOD, the photocurrent showed a significant decline (Fig. 3A, green curve), which could be attributed to the nonconducting nature of enzyme. In Fig. 3B, the semicircle part represents the electron transfer resistance (R_{et}), which represented the restricted diffusion of the redox probe through the different layers. Except the addition of RGO reduced the impedance, the modification of PbS and GOD all enhanced the impedance, the results were in accord with Fig. 3A. The inset of Fig. 3B was the analog circuit of EIS, *Rs*, *Zw*, *Cdl* were the solution resistance, Warburg impedance, and the double layer capacitance, respectively. The detailed simulated data (via ZsimpWin software) were shown in Table S1 (Supporting Information). As depicted in Fig. 3C, the on-off-on photocurrent circles within 440 s demonstrated that the fabricated PEC sensing platform have good signal output stability.

3.3. Optimization of experimental conditions for PEC detection

For the desired sensing PEC performance, some experimental details need to be optimized. The loading amount of PbS NPs have great impact on the PEC performance of PbS NPs/RGO/NiO NSAs, so we optimized the modification amount of PbS NPs by controlling successive ionic layer adsorption and reaction (SILAR) cycles. As shown in Fig. S2 (Supporting Information), in the beginning the photocurrent response of PbS NPs/RGO/NiO NSAs enhanced with the increasing of SILAR cycles, when the cycles excess 4 the photocurrent response decreased instead, this was due to the excess PbS NPs though enhanced light harvest but also greatly increased the electron transfer resistance. Hence, 4 SILAR cycles were selected for the PbS NPs modification.

3.4. Characterization of the proposed sensing platform for H_2O_2 and glucose analysis

Under optimized conditions, the analytical performance of the fabricated PEC biosensor for H_2O_2 and glucose detection were indicated via the linear regression equation. As depicted in Fig. 4A, it could be seen from the inset that the photocurrents increased with the increment of the concentrations of H_2O_2, and the photocurrents also linearly increased against the logarithm of H_2O_2 concentrations in the dynamic range of 0–100 mM. The limit of detection (LOD) was estimated to be 0.018 mM (S/N = 3). The linear regression equation for H_2O_2 detection was $\Delta I\ (\mu A) = -1.465 \lg c + 1.35$, and with a correlation coefficient (R^2) = 0.9820. The photoelectrochemical catalysis of RGO/NiO NSAs towards H_2O_2 can be described as follows: $NiO + OH^- - e^- \rightarrow NiOOH$; $2NiOOH + H_2O_2 \rightarrow 2NiO + 2H_2O + O_2$. Fig. 4B depicted the selectivity performance of the proposed H_2O_2 biosensor. As shown in the figure,

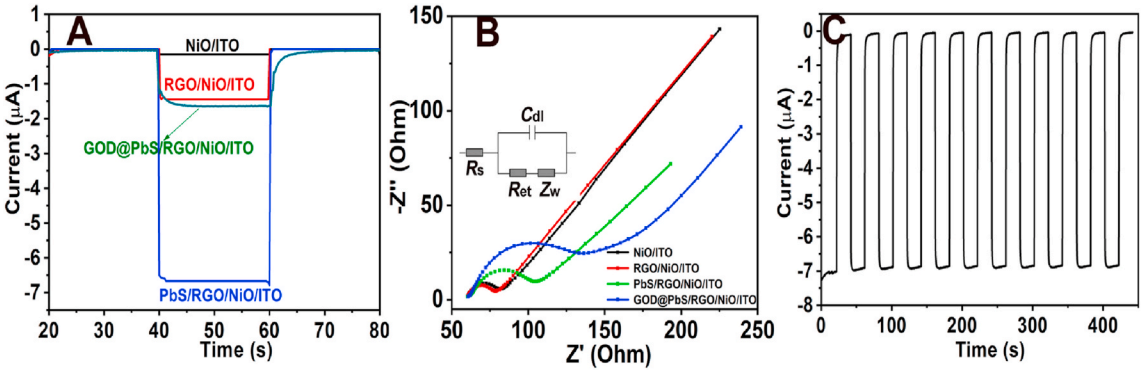

Fig. 3. (A) The photocurrent responses of NiO NSAs, RGO/NiO NSAs, PbS NPs/RGO/NiO NSAs and GOD@PbS NPs/RGO/NiO NSAs electrode, respectively. And (B) its corresponding EIS Nyquist plots (inset is the simulated equivalent circuit of EIS). (C) The PEC responses of the PbS NPs/RGO/NiO NSAs electrode under several "on-off" irradiation cycles for 440 s (bias voltage is 0 V).

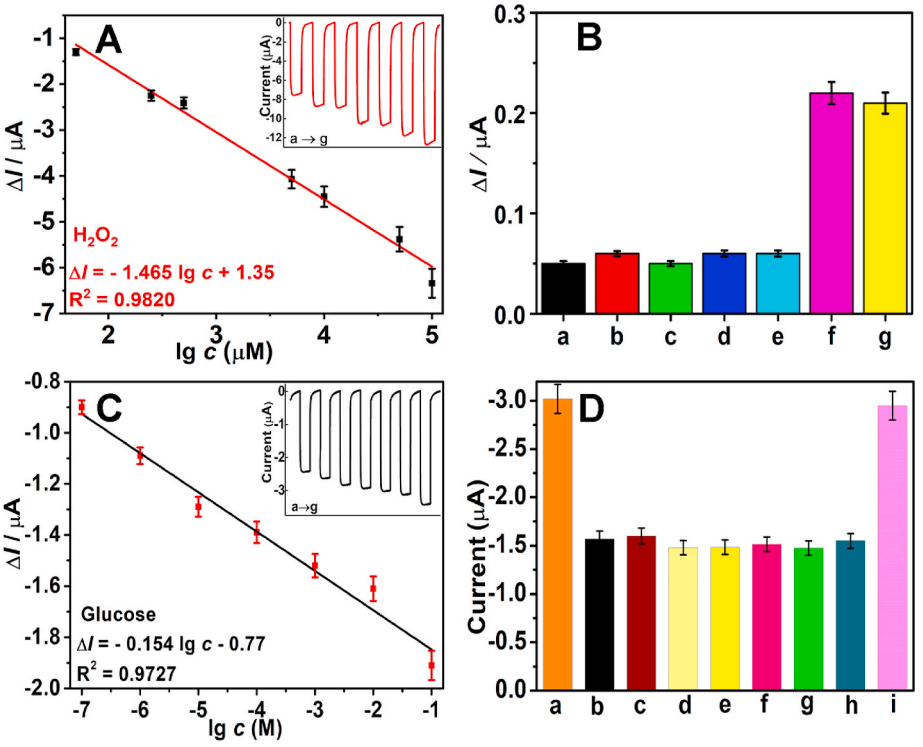

Fig. 4. (A) The photocurrent response ($\Delta I = I–I_0$, I_0 and I are the photocurrent of PbS NPs/RGO/NiO NSAs electrode before and after reaction with H_2O_2, respectively.) of the PbS NPs/RGO/NiO NSAs electrode vs. -log c_{H2O2}. Inset is the corresponding photocurrent response for different concentrations of H_2O_2 (a→g: 0.05, 0.25, 0.5, 5, 10, 50, 100 mM). The bias voltage is 0 V. (B) Effect of added interfering substances: (a) 0.1 mM Na_2SO_4, (b) 0.1 mM KCl, (c) 0.1 mM NaCl, (d) 0.1 mM glucose, (e) 0.1 mM dopamine, (f) 0.1 mM H_2O_2 and (g) 0.1 mM H_2O_2 + all other interfering substances. (C) The photocurrent increase of ($\Delta I = I - I_0$, with I_0 and I being the photocurrent responses of GOD@PbS NPs/RGO/NiO NSAs electrode before and after incubation with glucose, respectively.) of the GOD@PbS NPs/RGO/NiO NSAs electrode vs. -log $c_{glu.}$ Inset is the corresponding photocurrent response for different concentrations of glucose (a→g: 0.1, 0.01, 1×10^{-3}, 1×10^{-4}, 1×10^{-5}, 1×10^{-6}, 1×10^{-7} M). (D) The tested substances in turn are (a) 1 mM glucose , (b) 1 mM NaCl , (c) 1 mM ascorbic acid, (d) 1 mM urea, (e) 1 mM dopamine, (f) 1 mM lysine, (g) 1 mM L-histidine , (h) 1 mM cysteine and (i) 1 mM glucose + all other interfering substances. All the error bars represent the standard deviations of the three experiments.

only with the presence of H_2O_2 the PEC signal could have a big enhancement, which indicated the high selectivity of this biosensor.

Fig 4C presented the fabricated self-powered glucose PEC biosensor photocurrent responses toward the concentrations of glucose. The photocurrents linearly increased against the logarithm of glucose concentrations in a certain range of 0.1–1 × 10^{-7} M (LOD: 5.3 × 10^{-8} M). Meanwhile, the linear regression equation of this self-powered PEC biosensor conforms to the following equations: ΔI (μA) = −0.154 lg c - 0.77 (R^2 = 0.9727). The inset of Fig. 4C (a→g) was the corresponding photocurrent responses of the logarithm of glucose concentrations. Fig. 4D depicted the selectivity of the self-powered PEC biosensor for glucose analysis, as can be seen from the picture, with the presence of glucose (Fig 4Da and 4Di) the photocurrent were much higher than the samples without it, indicating the selectivity of this PEC biosensor was acceptable.

What's more, the analytical performance of the designed PEC biosensor for H_2O_2 and glucose detection were also compared with many previously works. As depicted in Table S2 (H_2O_2 detection comparison) and Table S3 (glucose detection comparison), the PbS NPs/RGO/NiO NSAs and GOD@PbS NPs/RGO/NiO NSAs self-powered sensing platform exhibited a wide detection range as well as a low LOD, which proved the promising future of the proposed sensing platform.

Reproducibility is an important indicator to evaluate a sensing platform. Herein, the reproducibility of the proposed self-powered PEC sensing platform was evaluated via intra-assay and inter-assay relative standard deviation (RSD). The intra-assay of PbS NPs/RGO/NiO NSAs sensing platform was operated via measuring one electrode five times with 5 mM and 15 mM H_2O_2, for which the obtained RSD value were 4.9% and 4.5%. While for the inter-assay, five of the proposed electrodes were used to detect 5 mM and 15 mM H_2O_2 under exactly the same conditions, the obtained RSD were 5.1% and 4.7%. In the same way, the intra-assay and inter-assay of GOD@PbS NPs/RGO/NiO NSAs electrode for 5 mM and 15 mM glucose were tested. For the intra-assay analysis the RSD were 3.3% and 4.3%, while for the inter-assay analysis the obtained RSD were 4.1% and 3.7%, respectively. The obtained results indicated acceptable reproducibility of the designed sensing platform for both the H_2O_2 and glucose monitoring.

3.5. *Real samples analysis*

In order to prove the practicability of the PbS NPs/RGO/NiO NSAs and GOD@PbS NPs/RGO/NiO NSAs sensing platform in conventional analysis, the proposed sensing platforms were used to detect the diluted H_2O_2 disinfectant solutions and real human serum samples (offered by local hospital, serum was diluted with 0.1 M Tris-HCl), respectively. The results of the proposed PEC sensing platform for H_2O_2 and glucose detection were compared with those obtained via commercialized H_2O_2 assay kit and glucometer, respectively. As shown in Table 1, the diluted H_2O_2 disinfectant samples and diluted serum samples with various concentrations were measured. The results of RSDs and the recoveries of both the diluted H_2O_2 disinfectant and human serum have acceptable precision and accuracy, which indicated the promising potential of the proposed sensing platform for biological analysis.

4. Conclusions

Inspired by that the H_2O_2 is the by-product of glucose enzymolysis, a cheap, sensitive and self-powered sensing platform was established for the in vitro measurement of H_2O_2 and glucose. NiO NSAs with excellent photocatalytic properties for H_2O_2, while the addition of RGO and PbS NPs can accelerate the electron transfer rate and enhance the light harvest efficiency. The proposed PbS NPs/RGO/NiO NSAs heterostructure is prepared layer by layer, and with one more step (addition of GOD), the proposed sensing platform can realize the detection conversion between H_2O_2 and glucose. We believe the design idea of sensitive, rapid, self-powered and function-switchable sensing platform would pave a new way for the design of biosensors in routine analysis.

CRediT authorship contribution statement

Qingzhi Han: Conceptualization, Data curation, Investigation, Methodology, Formal analysis, Writing - original draft, preparation. **Hanyu Wang:** Data curation, Writing - review & editing. **Dan Wu:**

Table 1
Comparison of analytical results for diluted H_2O_2 disinfectant and human serum samples via the proposed PEC sensing platform by using H_2O_2 assay kit and glucometer as the reference method, respectively.

Sample	Add (mM)	Reference Method (mM)	PEC Found (mM)	RSD, $n = 5$ (%)	Recovery (%)
H_2O_2 disinfectant	0.0	2.3	2.4	4.4	104.3
	3.0	5.4	5.3	3.9	98.15
	5.0	7.2	7.5	3.6	104.2
Human serum	0.0	1.1	1.2	4.3	109.1
	1.0	2.0	2.1	4.1	105.0
	3.0	4.2	4.3	3.2	102.4

Writing - review & editing, Funding acquisition, Supervision, Validation, Supervision, Funding Acquisition. **Qin Wei:** Funding acquisition, Supervision, Validation.

Declaration of competing interest

The authors declare that they have no known competing financial interests or personal relationships that could have appeared to influence the work reported in this paper.

Acknowledgements

We thank the financial support from the Young Taishan Scholars Program of Shandong Province (tsqn201009124), National Natural Science Foundation of China (21775054), Project of "20 items of University" of Jinan (2019GXRC018) as well as the National Key Scientific Instrument and Equipment Development Projects of China (21627809).

Appendix A. Supplementary data

Supplementary data to this article can be found online at https://doi.org/10.1016/j.bios.2020.112803.

References

Chi, H., Han, Q., Chi, T., Xing, B., Ma, N., Wu, D., Wei, Q., 2019. Biosens. Bioelectron. 132, 1–7.
Dai, W.X., Zhang, L., Zhao, W.W., Yu, X.D., Xu, J.J., Chen, H.Y., 2017. Anal. Chem. 89 (15), 8070–8078.
dos Santos, G.K.C., da Silva, F.G.S., Yotsumoto Neto, S., dos Santos, W.T.P., de Cássia Silva Luz, R., Damos, F.S., 2018. Electroanalysis 30 (8), 1750–1756.
Gong, M., Zhou, W., Tsai, M.C., Zhou, J., Guan, M., Lin, M.C., Zhang, B., Hu, Y., Wang, D. Y., Yang, J., Pennycook, S.J., Hwang, B.J., Dai, H., 2014. Nat. Commun. 5 (1), 4695.
Grattieri, M., Minteer, S.D., 2018. ACS Sens. 3 (1), 44–53.
Han, Q., Wang, H., Qi, Y., Wu, D., Wei, Q., 2019. Nanoscale Adv 1 (11), 4313–4320.
Han, Q., Wang, R., Xing, B., Chi, H., Wu, D., Wei, Q., 2018. Biosens. Bioelectron. 106, 7–13.
Jeevitha, G., Abhinayaa, R., Mangalaraj, D., Ponpandian, N., Meena, P., Mounasamy, V., Madanagurusamy, S., 2019. Nanoscale Adv 1 (5), 1799–1811.
Kang, Z., Gu, Y., Yan, X., Bai, Z., Liu, Y., Liu, S., Zhang, X., Zhang, Z., Zhang, X., Zhang, Y., 2015. Biosens. Bioelectron. 64, 499–504.
Katz, E., Bückmann, A.F., Willner, I., 2001. Self-powered enzyme-based biosensors. J. Am. Chem. Soc. 123 (43), 10752–10753.
Khot, K.V., Mali, S.S., Mane, R.M., Patil, P.S., Hong, C.K., Kim, J.H., Heo, J., Bhosale, P. N., 2015. J. Mater. Sci. Mater. Electron. 26 (9), 6897–6906.
Li, Q., Li, X., Wageh, S., Al-Ghamdi, A.A., Yu, J., 2015. Adv. Energy Mater. 5 (14), 1500010.
Li, X., Jiang, C., Zhao, F., Lan, L., Yao, Y., Yu, Y., Ping, J., Ying, Y., 2019. Nanomater. Energy 61, 78–85.
Liu, J., Li, Y., Ke, J., Wang, S., Wang, L., Xiao, H., 2018. Appl. Catal., B 224, 705–714.
Liu, X.L., Zhao, Y., Ma, S.X., Zhu, S.W., Ning, X.J., Zhao, L., Zhuang, J., 2019. ACS Sens. 4 (11), 3056–3065.
Luo, J., Wang, Z., Xu, L., Wang, A.C., Han, K., Jiang, T., Lai, Q., Bai, Y., Tang, W., Fan, F. R., Wang, Z.L., 2019. Nat. Commun. 10 (1), 5147.
Majdecka, D., Draminska, S., Janusek, D., Krysinski, P., Bilewicz, R., 2018. Biosens. Bioelectron. 102, 383–388.
Mukherjee, S., Jana, S., Sinha, T.K., Das, S., Ray, S.K., 2019. Nanoscale Adv 1 (8), 3279–3287.
Nardi, K.L., Yang, N., Dickens, C.F., Strickler, A.L., Bent, S.F., 2015. Adv. Energy Mater. 5 (17), 1500412.
Ouyang, B., Chang, C., Zhao, L.D., Wang, Z.L., Yang, Y., 2019. Nanomater. Energy 66, 104111.
Petromichelaki, E., Gagaoudakis, E., Moschovis, K., Tsetseris, L., Anthopoulos, T.D., Kiriakidis, G., Binas, V., 2019. Nanoscale Adv 1 (5), 2009–2017.
Sun, X., Zhang, H., Hao, S., Zhai, J., Dong, S., 2019. ACS Sens. 4 (10), 2631–2637.
Wang, Y., Tang, J., Peng, Z., Wang, Y., Jia, D., Kong, B., Elzatahry, A.A., Zhao, D., Zheng, G., 2014. Nano Lett. 14 (6), 3668–3673.
Wang, Y., Zhang, L., Cui, K., Ge, S., Zhao, P., Yu, J., 2019. ACS Appl. Mater. Interfaces 11 (5), 5114–5122.
Wilson, R., Turner, A.P.F., 1992. Biosens. Bioelectron. 7 (3), 165–185.
Wu, F., Li, C., Yin, Y., Cao, R., Li, H., Zhang, X., Zhao, S., Wang, J., Wang, B., Xing, Y., Du, X., 2019. Adv. Mater. Technol. 4 (1), 1800216.
Xiang, Q., Lang, D., Shen, T., Liu, F., 2015. Appl. Catal., B 162, 196–203.
Yu, Z., Li, H., Zhang, X., Liu, N., Zhang, X., 2015. Talanta 144, 1–5.
Zeng, R., Zhang, L., Su, L., Luo, Z., Zhou, Q., Tang, D., 2019. Biosens. Bioelectron. 133, 100–106.
Zhang, J., Tu, L., Zhao, S., Liu, G., Wang, Y., Wang, Y., Yue, Z., 2015. Biosens. Bioelectron. 67, 296–302.
Zhang, M., Zhang, Z., Xu, Y., Wen, Z., Ding, C., Guo, Y., Wang, K., 2020. Biosens. Bioelectron. 156, 112135.
Zhao, K., Yan, X., Gu, Y., Kang, Z., Bai, Z., Cao, S., Liu, Y., Zhang, X., Zhang, Y., 2016. Small 12 (2), 245–251.